

# Learning Image-Text Matching with Optimal Partial Transport

Zhengxin Pan  
Zhejiang University  
panzx@zju.edu.cn

Haishuai Wang  
Zhejiang University  
haishuai.wang@zju.edu.cn

Fangyu Wu  
Xi'an Jiaotong-Liverpool University  
Fangyu.wu02@xjtlu.edu.cn

Bailing Zhang  
NingboTech University  
bailing.zhang@nit.zju.edu.cn

Jiajun Bu  
Zhejiang University  
bjj@zju.edu.cn

Hongyang Chen  
Zhejiang Lab  
dr.h.chen@ieee.org

## Abstract

Cross-modal matching, a fundamental task in bridging vision and language, has recently garnered substantial research interest. Despite the development of numerous methods aimed at quantifying the semantic relatedness between image-text pairs, these methods often fall short of achieving both outstanding performance and high efficiency. In this paper, we propose the crOSS-Modal sInkhorn maTching (OMIT) network as an effective solution to effectively improving performance while maintaining efficiency. Rooted in the theoretical foundations of Optimal Transport, OMIT harnesses the capabilities of Cross-modal Mover’s Distance to precisely compute the similarity between fine-grained visual and textual fragments, utilizing Sinkhorn iterations for efficient approximation. To further alleviate the issue of redundant alignments, we seamlessly integrate partial matching into OMIT, leveraging local-to-global similarities to eliminate the interference of irrelevant fragments. We conduct extensive evaluations of OMIT on two benchmark image-text retrieval datasets, namely Flickr30K and MS-COCO. The superior performance achieved by OMIT on both datasets unequivocally demonstrates its effectiveness in cross-modal matching. Furthermore, through comprehensive visualization analysis, we elucidate OMIT’s inherent tendency towards focal matching, thereby shedding light on its efficacy. Our code is publicly available at <https://github.com/ppanzx/OMIT>.

## 1. Introduction

This study delves into the essential task of image-text matching, at the intersection of vision and language, with the goal of establishing semantic connections between visual and textual data. The conventional method for image-text matching, known as Visual Semantic Embedding [17, VSE], involves embedding data from different modalities into a single vector

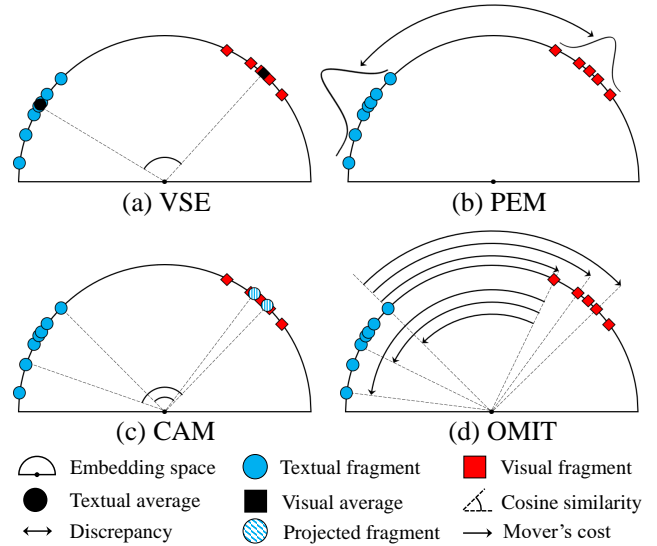


Figure 1. Comparison between different image-text matching methods. (a) VSE directly calculates the cosine similarity between two average vectors. (b) PEM substitutes the cosine similarity with the divergence of parametric distributions. (c) CAM measures the average cosine similarities between query fragments and their projections. (d) OMIT regards the Cross-modal Mover’s Distance as the dissimilarity.

in a common representation space. This arrangement ensures that semantically coherent samples are positioned adjacently, as depicted in Figure 1 (a). Despite VSE’s notable improvements, recent research has underscored the insufficiency of representing images or captions with singular vectors due to inherent ambiguity [43]. Consequently, researchers have shifted their focus toward a more fine-grained form of cross-modal matching.

Existing fine-grained matching methods can be broadly categorized into two groups: the cross-attention-based method (CAM) such as [27], and the probabilistic-

embedding-based method (PEM) like [12]. PEM assumes that each sample corresponds to a Gaussian distribution within the common space. By incorporating an additional covariance, it extends the semantic information of the samples, leading to more comprehensive representations, as illustrated in Figure 1 (b). The overall similarity between an image-text pair is then defined by measuring the distance between these two distributions. However, relying solely on the distribution assumption may produce degenerate results due to the presence of inter-dependency among local fragments and the lack of semantic continuity.

CAM assumes that an image can adequately depict a caption when the image-caption pair is semantically aligned, it also gauges the probability of textual fragment absence in the image through reconstruction error. Specifically, CAM projects each sample into a diverse feature set and computes the average projection similarity between the two feature sets, as depicted in Figure 1(c). CAM effectively discovers shared semantics, thus presents improved performance, however, as discussed in [36], it is susceptible to redundant alignments and low efficiency. In addition, CAM fails to consider the relative significance among textual fragments, leading to limited performance.

Taking into account the simultaneous importance of both visual and textual fragments, we extend the concept of cross-attention to Optimal Transport (OT). As depicted in Figure 1(d), OT endeavors to minimize the cumulative cost of "transporting" embeddings from one modality to their corresponding embeddings in the other modality, describing a good metric for measuring the distance between two discrete distributions. The bidirectional nature of OT is reflected in the resulting transport plan, which accounts for the constraints of visual and textual significance. To address the issue of low computational efficiency in OT, we leverage the Sinkhorn-Knopp algorithms [14] to approximate Earth Mover's Distance with the Sinkhorn distance, enabling both effective and efficient retrieval. Our experiments show that Sinkhorn distance serves as a more appropriate metric for capturing semantic correlations than current counterparts.

Additionally, to address the problem of redundant alignments, we introduce the concept of partial matching into OT, resulting in Optimal Partial Transport (OPT). In comparison to OT, OPT discards the requirement for complete correspondence and relaxes the marginal constraints, thereby enhancing its resilience to the challenges posed by noisy fragments. Specifically, we leverage the global embeddings as "dustbins" for matching, enhancing the alignments with common semantics and eliminating irrelevant alignments. Building on OPT, we introduce the crOss-Modal sInkhorn maTching (OMIT) network. Remarkably, OMIT demonstrates superior capabilities in uncovering latent visual-semantic alignments, surpassing the performance of current state-of-the-art (SOTA) methods on two cross-modal retrieval benchmarks.

In summary, our contributions can be succinctly outlined as follows:

(1) We address measuring the similarity between cross-modal pairs by harnessing the power of Optimal Transport. We demonstrate that the Sinkhorn distance, a numerical approximation of the Earth Mover's Distance, efficiently and effectively captures semantic correlations between visual and textual grained embeddings.

(2) We introduce OMIT for cross-modal retrieval, using cross-modal local-to-global correlations as a criterion to effectively filter out redundant alignments. Our OMIT achieves SOTA results on two benchmark datasets, i.e., MSCOCO [30] and Flickr30K [52], demonstrating its effectiveness of partial matching.

(3) Our experiments shed light on the optimal transport plan generated by OMIT, showcasing its more focused attention compared to the counterpart generated by CAM. These findings align with existing literature [53], further validating the efficacy of our approach.

## 2. Related Works

**Cross-modal Matching.** An initial milestone in cross-modal matching was set by naïve VSE. This method hinges on merging local embeddings into a global embedding via various aggregation techniques. Examples include plain mean pooling [16, 17], self-attention layers [44], GCN [28], or learnable pooling [9]. Subsequently, pairwise global embedding similarity is calculated using cosine similarity for ranking. However, VSE exhibits shortcomings in reasoning implicit associations and managing ambiguity. To address these limitations, PEM enhances VSE by employing probabilistic representations. It establishes a richer embedding space, where each image or text is represented as a Gaussian distribution, and similarity is computed as the divergence between these distributions. Subsequent research endeavors have further bolstered the efficacy of PEM through advancements in geometric spaces [46], multifaceted relationships [46], and superior metrics [1]. Despite these efforts, the enhancements stemming from probabilistic embedding are modest, as evidenced by findings in [12]. Consequently, the representation of data with parametric distributions inherently exhibits limitations.

A distinctive approach, CAM, aligns discrete embeddings by leveraging set algebra guidance. It gauges whether a data sample (e.g., image) embodies the concept of a fragment from the other modality (e.g., token) by assessing the reconstruction similarity between the textual embedding and visual feature sets. Nevertheless, recent studies [36] have illuminated that CAM fundamentally optimizes the coding distance and grapples with redundant alignment issues. In response, strategies to address redundancy have emerged, such as IMRAM [8], which iteratively refines coarse corre-

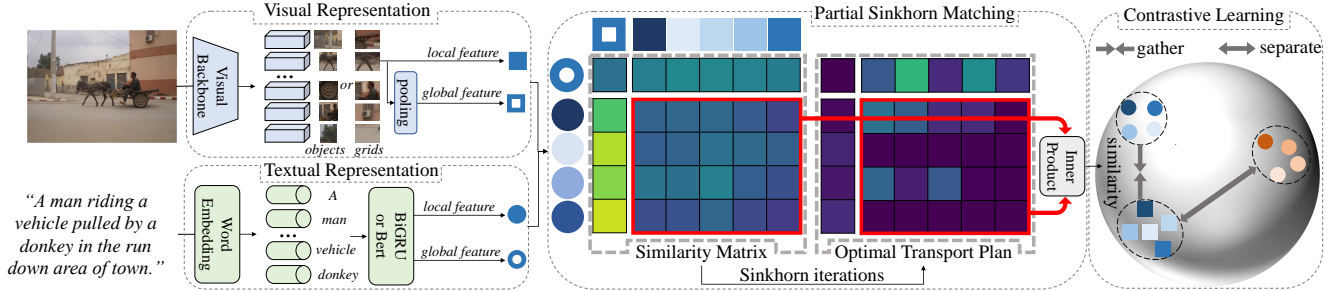


Figure 2. Overview of the OMIT. We begin by projecting the caption and image to the common space using textual and visual encoders, resulting in cross-modal fragments. Next, we employ the partial matching and calculate the Sinkhorn distance between fragments in the Partial Sinkhorn Matching module. Finally, we leverage the contrastive loss to group relevant fragments and distinguish irrelevant fragments.

spendences using cross-attention layers, NAAF [53], which introduces a negative attention module to amplify the significance of matched fragments, and CHAN [36], which deconstructs the cross-attention mechanism with a coding framework to mitigate surplus alignments. Despite these advances, CAM’s asymmetry and sub-optimality stem from its limited robustness in facilitating complete mutual expression. To surmount these challenges, our proposed OMIT adeptly sidesteps the issues elucidated above.

**Optimal Transport.** The lineage of research on Optimal Transport (OT) traces back to the 18th-century Monge problem, which aimed to transfer a heap of sand to a target pile of specific shape with minimal effort [38]. The minimal cost, also known as the Earth Mover’s Distance (EMD) or Wasserstein distance, has found extensive applications in Computer Vision and Natural Language Processing for addressing matching challenges. For instance, [41] utilized EMD to match the signatures of two images for image retrieval, [26] calculated the EMD between the embedded words of two text documents to indicate their dissimilarity. [3] minimized the EMD between real data distribution and a generator’s distribution.

The endeavor to extend OT from single-modality to cross-modality is a burgeoning field that has recently captivated researchers. [10] approached cross-modal matching problems from the perspective of graph matching, utilizing OT to simultaneously match nodes and edges between two heterogeneous graphs. [45] aligned the graph of raw data and the counterpart graph in a graph dictionary with OT, thus achieving powerful feature embedding. [56] deviated from the graph matching formulation and introduced a simple method to align image patches with text tokens using empirical approximate EMD. This innovation inspired our goal to directly aligning cross-modal fragments. Distinguishing itself from the approach in [56], our work leverages the precision of the Bregman algorithm [6] for iterative EMD approximation, avoiding sub-optimal solution.

While several works have utilized OT for cross-modal matching, they often focus solely on the full correspondence

between local fragments, disregarding the fact that many alignments lack meaningful associations. To the best of our knowledge, we are the first to address this limitation by relaxing the constraint of full correspondence and enhancing the capabilities of OT through partial matching.

### 3. Approach

#### 3.1. Image-text Matching with Optimal Transport

Without loss of generality, an image can be represented granularly by a set of local embeddings denoted as  $\mathcal{V}_m = \{v_i |_{i=1}^{K_m}\}$ , while a caption is represented as  $\mathcal{T}_n = \{t_j |_{j=1}^{L_n}\}$ . In this context,  $m$  and  $n$  index the dataset,  $v_i \in \mathbb{R}^d$  and  $t_j \in \mathbb{R}^d$  represent the  $d$ -dimensional embeddings of an image sub-region/patch and a text token, respectively. Furthermore,  $K_m$  and  $L_n$  indicate the number of fragments in the image and the caption, respectively. Optimal Transport (OT) computes the Cross-modal Mover’s Distance, denoted as  $\mathcal{D}_{OT}$ , between an image  $\mathcal{V}_m$  and a caption  $\mathcal{T}_n$  as a measure of their semantic similarity. The formulation of this distance is as follows:

$$\mathcal{D}_{OT}(\mathcal{V}_m, \mathcal{T}_n) = \min_{\Omega \in \mathcal{U}(\alpha, \beta)} \langle \Omega, \mathbf{C} \rangle := \sum_{i=1}^{K_m} \sum_{j=1}^{L_n} \omega_{ij} c_{ij}$$

$$\text{subject to } \Omega \mathbf{1}_{L_n} = \alpha, \Omega^\top \mathbf{1}_{K_m} = \beta, \Omega \in \mathbb{R}_+^{K_m \times L_n} \quad (1)$$

where  $\alpha$  and  $\beta$  denote marginal distributions of visual fragments and textual fragments, respectively. For simplicity, we treat all fragments within the same modality equally, thus setting  $\alpha_i = \frac{1}{K_m}$  and  $\beta_j = \frac{1}{L_n}$ .  $\mathbf{C} \in \mathbb{R}_+^{K_m \times L_n}$  is the cost matrix, where each element  $c_{ij}$  represents the distance between  $v_i$  and  $t_j$ . In this case, we choose  $c_{ij}$  to be twice the  $l_2$  distance:  $c_{ij} = 1 - v_i^\top t_j$ . The matrix  $\Omega$  corresponds to one of the transport plans denoted as  $U(\alpha, \beta)$ , which must satisfy the marginal conditions in Equation 1.  $\omega_{ij}$  refers to an individual element of  $\Omega$ .

However, directly optimizing Equation 1 can be computationally intensive. To overcome this challenge, we adopt

an approach proposed in [14], which introduces an entropic constraint on  $\Omega$  and constrains the feasible solution space, resulting in efficient optimization. As a result, we approximate the CMD by utilizing the Sinkhorn distance  $\mathcal{D}_S$ , which is given by:

$$\mathcal{D}_S(\mathcal{V}_m, \mathcal{T}_m) = \min_{\Omega \in \mathcal{U}(\hat{\alpha}, \hat{\beta})} \langle \Omega, \mathbf{C} \rangle - \lambda H(\Omega) \quad (2)$$

where  $H(\Omega) = -\sum_{i=1}^{K_m} \sum_{j=1}^{L_n} \omega_{ij} (\log \omega_{ij} - 1)$  is the entropy term, and  $\lambda \geq 0$  is the scalar factor that balances the convergence speed and proximity to the optimal solution. Mathematically, when  $\lambda$  is sufficiently small, the solution to Equation 2 is equivalent to the optimal plan derived from Equation 1. The unique solution  $\Omega^*$  of Equation 2 can be obtained by iteratively projecting the Gibbs kernel  $\xi = e^{-\frac{\mathbf{C}}{\lambda}}$  to normalize either its rows or columns using Sinkhorn iterations [4, 14]:

$$\begin{aligned} \Omega^{(2t+1)} &= \text{diag}\left(\frac{\alpha}{\Omega^{(2t)} \mathbf{1}_{L_n}}\right) \Omega^{(2t)} \\ \Omega^{(2t+2)} &= \Omega^{(2t+1)} \text{diag}\left(\frac{\beta}{\Omega^{(2t+1)\top} \mathbf{1}_{K_m}}\right) \\ \text{Initialize } \Omega^{(0)} &= \xi \end{aligned} \quad (3)$$

where  $t$  denotes the iteration steps. Equation 3 will converge with several steps, ensuring efficient matching.

### 3.2. Improving OT with Partial Matching

One evident challenge in vanilla OT for image-text matching is the presence of redundant alignments. These alignments refer to region-word pairs that lack semantic coherence but contribute significantly to the overall similarity. Since an image and a sentence cannot fully capture each other's content [50], there are instances where certain objects in the image do not correspond to any words in the sentence. When employing naïve OT for matching, these pairs are inevitably included in the overall similarity computation, resulting in unwanted disturbances. A straightforward solution to this problem is to establish a suitable threshold for each image-text pair, filtering out alignments with similarities below the threshold. However, determining the appropriate threshold for each fragment requires fragment-specific considerations, making manual tuning a time-consuming and labor-intensive process.

Inspired by the concept of partial matching in Optimal Partial Transport, we have discovered that re-weighting is a more appropriate and efficient approach compared to thresholding. Instead of filtering out redundant alignments, we assign them a small weight, thereby reducing their interference in the matching process. To achieve this, we introduce additional visual global embedding  $\bar{v}$  and textual embedding  $\bar{t}$  as "dustbins" for matching. In this manner, we redefine the

optimal transport plan as follows:

$$\begin{aligned} \hat{\Omega}^* &= \arg \min_{\hat{\Omega} \in \mathcal{U}(\hat{\alpha}, \hat{\beta})} \langle \hat{\Omega}, \hat{\mathbf{C}} \rangle \\ &= \arg \min_{\hat{\Omega} \in \mathcal{U}(\hat{\alpha}, \hat{\beta})} \left\langle \begin{bmatrix} \Omega_g & \Omega_{gv} \\ \Omega_{gt} & \Omega \end{bmatrix}, \begin{bmatrix} \mathbf{C}_g & \mathbf{C}_{gv} \\ \mathbf{C}_{gt} & \mathbf{C} \end{bmatrix} \right\rangle \\ \text{subject to } &\hat{\Omega} \mathbf{1}_{L_n+1} = \hat{\alpha}, \hat{\Omega}^\top \mathbf{1}_{K_m+1} = \hat{\beta}, \\ &\hat{\Omega} \in \mathbb{R}_+^{(K_m+1) \times (L_n+1)} \end{aligned} \quad (4)$$

The symbols superscript with  $\hat{\cdot}$  denote the extended version of their original matrix. For instance,  $\hat{\mathbf{C}}$  extends  $\mathbf{C}$  by incorporating auxiliary components such as the cost between dustbins  $\mathbf{C}_g$ , the cost between visual dustbin and textual fragments  $\mathbf{C}_{gv}$  and the cost between textual dustbin and visual fragments  $\mathbf{C}_{gt}$ . Equation 4 can be solved using Sinkhorn iterations formulated in Equation 3. The overall similarity between the image  $\mathcal{V}_m$  and the caption  $\mathcal{T}_m$  is defined as:

$$\mathcal{S}_{OT}(\mathcal{V}_m, \mathcal{T}_m) = 1 - \mathcal{D}_{OT} = \langle \Omega^*, \mathcal{V}_m \mathcal{T}_m^\top \rangle \quad (5)$$

In above equation, we consider only the optimal transport plan between local fragments to quantify the overall similarity. We discard the auxiliary parts such as  $\Omega_g^*$ ,  $\Omega_{gv}^*$ , and  $\Omega_{gt}^*$ . By doing so, we ensure that fragments irrelevant to the shared semantics correspond to the global dustbin, effectively eliminating their contribution to the overall similarity.

### 3.3. Cross-Modal Sinkhorn Matching

The OMIT framework comprises four components, as depicted in Figure 2. The Partial Sinkhorn Matching module has been primarily discussed earlier, and the remaining modules are described in detail below.

**Visual Representation.** We adopt two different types of visual features, namely grid feature [21] and region feature [2], for granular representation. For grid representation, we employ a CNN like ResNet-152 [19] or ResNeXT-101 [49] as the backbone (excluding the last pooling and linear layer) to capture image patches. Alternatively, to capture higher-level information such as objects within an image, we utilize the Faster-RCNN [40] equipped with Bottom-Up-and-Top-Down attention (BUTD) [2], which is pretrained on the Visual Genome dataset [25], to encode salient sub-regions. Following nonlinear transformations and normalization, the resulting grid or region features are considered as the visual fragments  $\{v_i\}_{i=1}^{K_m}$ . To obtain the global feature  $\bar{v}$ , we simply apply average pooling to the fragments.

**Text Representation.** To obtain the textual fragments  $\{t_j\}_{j=1}^{L_n}$ , we employ sequential networks such as BiGRU [13] or pretrained Bert [22] to contextualize dense word embeddings [37]. Each output from the sequential model represents a granular embedding  $t_j$ . Subsequently,

Table 1. Image-Text Retrieval Results of OMIT method on Flickr 30K and COCO 5K test set, using different visual and text backbones (denoted by **bold section title**). \*: Ensemble results of two models. † denotes results using post-processing techniques like DSL [11]. The best (in RSUM) are marked **bold** in **red**.

METHOD	TYPE	Flickr 30K Test set [52]							COCO 5K Test set [30]						
		IMG → TEXT			TEXT → IMG			RSUM ↑	IMG → TEXT			TEXT → IMG			RSUM ↑
		R@1	R@5	R@10	R@1	R@5	R@10		R@1	R@5	R@10	R@1	R@5	R@10	
<b>ResNet-152 [19] + BiGRU [13]</b>															
VSE++ [16]	VSE	52.9	80.5	87.2	39.6	70.1	79.5	409.8	41.3	71.1	81.2	30.3	59.4	72.4	355.7
PVSE [43]	PEM	59.1	84.5	91.0	43.4	73.1	81.5	432.6	45.2	74.3	84.5	32.4	63.0	75.0	374.4
PCME [12]	PEM	58.5	81.4	89.3	44.3	72.7	81.9	428.1	44.2	-	-	31.9	-	-	-
SBE [23]	CAM	61.8	85.5	91.1	46.1	74.8	83.3	442.6	47.2	74.8	84.1	33.8	63.1	74.7	377.7
ours	OMIT	67.6	90.6	95.2	52.5	79.3	86.6	<b>471.8</b>	46.7	76.9	87.0	35.9	65.4	76.7	<b>388.6</b>
<b>BUTD [2] + BiGRU [13]</b>															
SCAN* [27]	CAM	67.4	90.3	95.8	48.6	77.7	85.2	465.0	50.4	82.2	90.0	38.6	69.3	80.4	410.9
VSRN* [28]	VSE	71.3	90.6	96.0	54.7	81.8	88.2	482.6	53.0	81.1	89.4	40.5	70.6	81.1	415.7
CAAN [54]	VSE	70.1	91.6	97.2	52.8	79.0	87.9	478.6	52.5	83.3	90.9	41.2	70.3	82.9	421.1
IMRAM* [8]	CAM	74.1	93.0	96.6	53.9	79.4	87.2	484.2	53.7	83.2	91.0	39.7	69.1	79.8	416.5
SGRAF* [15]	CAM	78.4	94.6	97.5	58.2	83.0	89.1	500.8	55.8	83.0	91.0	42.0	72.4	82.1	426.3
VSE <sub>∞</sub> [9]	VSE	76.5	94.2	97.7	56.4	83.4	89.9	498.1	56.6	83.6	91.4	39.3	69.9	81.1	421.9
NAAF [53]	CAM	79.6	96.3	98.3	59.3	83.9	90.2	507.6	58.9	85.2	92.0	42.5	70.9	81.4	430.9
SBE [23]	PEM	77.8	94.0	97.5	57.5	84.0	90.0	500.8	58.8	84.9	91.5	41.1	72.0	82.4	430.7
HREM [18]	VSE	79.5	94.3	97.4	59.3	85.1	91.2	506.8	58.9	85.3	92.1	40.0	70.6	81.2	428.1
ours	OMIT	80.1	96.1	98.2	61.9	85.8	91.5	<b>513.5</b>	60.2	85.6	92.1	42.6	71.8	81.4	<b>433.8</b>
<b>BUTD [2] + BERT [22]</b>															
MMCA [48]	CAM	74.2	92.8	96.4	54.8	81.4	87.8	487.4	54.0	82.5	90.7	38.7	69.7	80.8	416.4
VSE <sub>∞</sub> [9]	VSE	81.7	95.4	97.6	61.4	85.9	91.5	513.5	58.3	85.3	92.3	42.4	72.7	83.2	434.3
TERAN* [34]	CAM	79.2	94.4	96.8	63.1	87.3	92.6	513.4	59.3	85.8	92.4	45.1	76.4	84.4	443.4
VSRN+++ [29]	VSE	79.2	94.6	97.5	60.6	85.6	91.4	508.9	54.7	82.9	90.9	42.0	72.2	82.7	425.4
CHAN [36]	CAM	80.6	96.1	97.8	63.9	87.5	92.6	518.5	59.8	87.2	93.3	44.9	74.5	84.2	443.9
HREM [18]	VSE	83.3	96.0	98.1	63.5	87.1	92.4	520.4	62.3	87.6	93.4	43.9	73.6	83.3	444.1
ours	OMIT	83.1	96.5	98.7	65.7	88.5	93.3	<b>525.8</b>	64.5	88.2	93.7	46.0	75.3	84.4	<b>452.0</b>
<b>ResNeXT-101(WSL) [33] + BERT [22]</b>															
VSE <sub>∞</sub> [9]	VSE	88.4	98.3	99.5	74.2	93.7	96.8	550.9	66.4	89.3	94.6	51.6	79.3	87.6	468.9
SBE [23]	PEM	88.8	98.5	99.6	74.3	94.0	96.7	551.9	69.1	90.7	95.6	52.1	79.6	87.8	474.9
ours	OMIT	91.0	99.0	99.9	78.1	95.2	97.6	<b>560.7</b>	69.0	90.7	95.5	54.0	80.4	88.3	<b>477.9</b>
<b>CLIP VIT-B/32 [39]</b>															
zero-shot CLIP [39]	VSE	78.9	94.9	98.2	58.8	83.5	90.0	504.3	50.1	74.9	83.4	30.4	56.0	66.9	361.7
fine-tuned CLIP	VSE	86.9	97.3	99.3	72.0	92.3	96.2	544.1	62.9	85.8	92.0	46.2	73.4	82.9	443.3
ours	OMIT	86.4	97.8	99.7	73.6	92.8	96.0	546.2	63.3	86.7	92.5	48.5	75.7	84.2	450.9
ours†	OMIT	93.9	99.1	99.6	76.6	93.9	97.1	<b>560.2</b>	72.1	89.3	93.9	50.1	75.9	84.3	<b>465.6</b>

we project  $t_j$  into the same space as  $v_i$  to enable subsequent matching. When using BERT, we adopt the **CLS** token as the global feature. For BiGRU, we compute the mean vector of the local embeddings to obtain the global feature.

**Objective.** Following previous works [16, 27, 28], we adopt a hinge-based triplet ranking loss with online hardest negative mining [16] to enforce that the similarity between a semantically consistent image-text pair is greater than that of an unrelated image-text pair by a margin  $\phi$ . The optimization

objective is defined by the following loss function:

$$\mathcal{L} = \sum_{m=1}^M \max_{n \neq m} [\phi + \mathcal{S}_{OT}(\mathbf{V}_m, \mathcal{T}_m) - \mathcal{S}_{OT}(\mathbf{V}_m, \mathcal{T}_n)]_+ + \sum_{n=1}^N \max_{m \neq n} [\phi + \mathcal{S}_{OT}(\mathbf{V}_n, \mathcal{T}_n) - \mathcal{S}_{OT}(\mathbf{V}_m, \mathcal{T}_n)]_+ \quad (6)$$

where  $M$  and  $N$  are the sizes of images and captions in the minibatch. The notation  $[\cdot]_+$  denotes the hinge function.

Data with the same index signifies semantic consistency, whereas different indices indicate a mismatched pair.

## 4. Experiments

Table 2. Image-Text Retrieval Results of the OMIT on MS-COCO 5-fold 1K test set.

METHOD	TYPE	IMG → TEXT			TEXT → IMG			RSUM ↑
		R@1	R@5	R@10	R@1	R@5	R@10	
<b>ResNet-152 + BiGRU</b>								
VSE++	VSE	64.6	90.0	95.7	52.0	84.3	92.0	478.6
PVSE	PEM	69.2	91.6	96.6	55.2	86.5	93.7	492.8
PCME	PEM	68.8	-	-	54.6	-	-	-
SBE	PEM	70.3	91.5	96.3	56.0	85.8	93.3	493.2
ours	OMIT	71.3	93.6	97.7	57.8	87.2	94.2	<b>501.9</b>
<b>BUTD + BiGRU</b>								
SCAN*	CAM	72.7	94.8	98.4	58.8	88.4	94.8	507.9
VSRN*	VSE	76.2	94.8	98.2	62.8	89.7	95.1	516.8
CAAN	VSE	75.5	95.4	98.5	61.3	89.7	95.2	515.6
IMRAM*	CAM	76.7	95.6	98.5	61.7	89.1	95.0	516.6
SGRAF*	CAM	79.6	96.2	98.5	63.2	90.7	96.1	524.3
VSE $\infty$	VSE	78.5	96.0	98.7	61.7	90.3	95.6	520.8
NAAF	CAM	78.1	96.1	98.6	63.5	89.6	95.3	521.2
HREM	VSE	80.0	96.0	98.7	62.7	90.1	95.4	522.8
ours	OMIT	80.4	96.0	98.6	63.8	90.1	95.6	<b>524.4</b>
<b>BUTD + BERT</b>								
MMCA	CAM	74.8	95.6	97.7	61.6	89.8	95.2	514.7
VSE $\infty$	VSE	79.7	96.4	98.9	64.8	91.4	96.3	527.5
TERAN*	CAM	80.2	96.6	99.0	67.0	92.2	96.9	531.9
VSRN+++*	VSE	77.9	96.0	98.5	64.1	91.0	96.1	523.6
CHAN	CAM	81.4	96.9	98.9	66.5	92.1	96.7	532.6
HREM	VSE	81.1	96.6	98.9	66.1	91.6	96.5	530.7
ours	OMIT	83.2	97.0	98.9	67.5	91.9	96.5	<b>535.1</b>
<b>ResNeXT-101(WSL) + BERT</b>								
VSE $\infty$	VSE	84.2	97.8	99.3	71.9	93.9	97.5	544.6
SBE	PEM	86.3	97.8	99.4	72.4	94.0	97.6	547.5
ours	OMIT	85.7	98.1	99.3	73.2	94.4	97.8	<b>548.5</b>
<b>CLIP VIT-B/32</b>								
zs CLIP	VSE	69.1	91.0	95.7	49.7	79.4	88.8	473.6
ft CLIP	VSE	80.8	96.2	98.2	66.3	91.0	96.4	528.8
ours	OMIT	81.6	96.7	98.6	68.2	91.7	96.2	<b>532.9</b>

### 4.1. Settings.

**Datasets.** We evaluate our approach on two benchmark image-text retrieval datasets, namely MS-COCO [30] and Flickr30K [52], to validate its effectiveness. MS-COCO consists of 123,287 images, each of which is manually captioned with five sentences. Following the protocols in [16], we split 113,287 images in MS-COCO for training, 5,000

for validation, and the remaining 5,000 for testing. Similarly, images in Flickr30K are divided into 29,769 training images, 1,014 validating images, and 1,000 testing images.

**Metrics.** We employ the commonly used evaluation measure,  $R@K$ , which measures the percentage of relevant items among the top-K retrieved items for a given query, to assess the performance of our models. We consider  $R@1$ ,  $R@5$ , and  $R@10$  for universal evaluation and use  $RSUM = R@1 + R@5 + R@10$  to compare overall performance between our method and others. All our results are reported on the test set using the model that performs best on the validation set. Notably, we do not report any integrated results by assembling two separated models but display the **single-model** results.

**Implementation details.** The OMIT model is meticulously optimized using the AdamW optimizer [32] with a weight decay of  $5e - 4$ . For the region feature, a batch size of 384 is utilized, while for the grid feature, a batch size of 128 is employed. where the initial 10 epochs adopt a learning rate of  $5e - 4$ , followed by the subsequent 5 epochs with a learning rate of  $5e - 5$ . The resolution for the input image is set to  $224 \times 224$ , the number of proposals for salient regions is set to 36. The values of  $\lambda$  and  $\phi$  are set to 0.02 and 0.05, respectively.  $\tau$  in Equation 4 is set to 0.1. The visual mask ratio is set to 0.4 for the region feature and 0.2 for the grid feature. Captions are randomly masked at a ratio of 0.1, replaced at a ratio of 0.02, and discarded at a ratio of 0.08. Consistent with prior work [16], the embedding dimension  $d$  is set to 1024. To address the issue of slow convergence in the ranking loss [47], we adopt the approach proposed in [9] and perform a warm-up phase for OMIT during the first epoch, without engaging in hard negative mining.

### 4.2. Comparison Results

Table 1 and Table 2 provide comprehensive comparisons of our OMIT with current state-of-the-art (SOTA) methods on three benchmarks. For fairness, we categorize the methods according to their backbones. Remarkably, across all datasets and backbones, our OMIT outperforms all other methods, achieving the highest  $RSUM$  score. Interestingly, all our text-to-image  $R@1$  scores are approximately 2% higher than those of current methods, likely because all our OMIT variants effectively harness the potential of visual backbones.

Specifically, when compared to baselines employing ResNet and BiGRU (first blocks), OMIT exhibits significant improvements of at least 29.2%, 10.9% and 8.7% over SOTA SBE in terms of  $RSUM$  on the Flickr30K, COCO 5K and COCO 5-fold 1K, respectively. Furthermore, when compared to methods utilizing region features such as SCAN, NAAF, and HREM (second and third blocks), OMIT achieves the best results at  $R@1$  and  $RSUM$  for both datasets under the same conditions of BUTD and Bi-

Table 3. Comparison of OMIT with other matching methods on the Flickr30K test set. The TIME denotes the overall computational time for matching total visual embeddings and textual embeddings.

TYPE	IMG → TEXT			TEXT → IMG			RSUM↑	TIME(s)↓
	R@1	R@5	R@10	R@1	R@5	R@10		
<b>ResNet-152 [19] + BiGRU [13]</b>								
VSE	59.6	85.3	90.6	44.5	74.5	83.2	437.8	9.48
PEM	60.2	85.8	91.4	46.6	74.7	83.6	442.3	<b>9.43</b>
CAM	67.4	91.1	95.3	50.5	78.5	86.8	469.7	42.55
OMIT	67.6	90.6	95.2	52.5	79.3	86.6	<b>471.8</b>	15.03
<b>BUTD [2] + BiGRU [13]</b>								
VSE	61.3	85.0	92.3	44.5	75.3	83.8	442.2	<b>10.91</b>
PEM	70.7	90.8	94.8	51.2	79.4	86.7	473.6	12.03
CAM	80.5	95.3	97.7	58.7	84.2	90.3	506.8	22.31
OMIT	80.1	96.1	98.2	61.9	85.8	91.5	<b>513.5</b>	16.93

GRU/Bert. Finally, when equipped with the more powerful visual encoder ResNeXT-101, along with a higher visual resolution (last blocks), OMIT achieves significant retrieval improvements and consistently outperforms counterparts such as VSE $\infty$  and SBE.

### 4.3. Ablation Study

**Compared With Other Matching Methods.** We conduct experiments to perform a fair comparison between our OMIT and other existing methods. To ensure fairness, we exclusively replace the Partial Sinkhorn Matching module with various alternatives. The results are presented in Table 3, where OMIT demonstrates the highest accuracy while remaining competitive in terms of efficiency. In particular, when compared to global embedding methods like VSE and PEM, OMIT exhibits noteworthy improvements in all effectiveness indicators, including  $R@1$  and  $RSUM$ , despite a slight decrease in efficiency. In contrast, when pitted against other more precise methods like CAM, OMIT not only improves retrieval efficiency but also achieves superior accuracy. This enhanced efficiency of OMIT can be attributed to its omission of the reconstruction process, while the rationale behind its improved accuracy will be expounded upon in subsequent sections.

**Analysis of Hyper-parameter  $\lambda$ .** We conduct ablation studies to investigate the impact of the hyper-parameter  $\lambda$  defined in Equation 2. The upper part of Figure 3 illustrates that as  $\lambda$  decreases, Sinkhorn distance approaches the CMD, leading to a notable improvement in performance that eventually converges to the optimal result. This finding demonstrates that CMD is an effective metric for capturing semantic similarity.

Furthermore, we present a visualization of the optimal transport in the lower part of Figure 3, which offers insights into the contribution of the alignment between the word

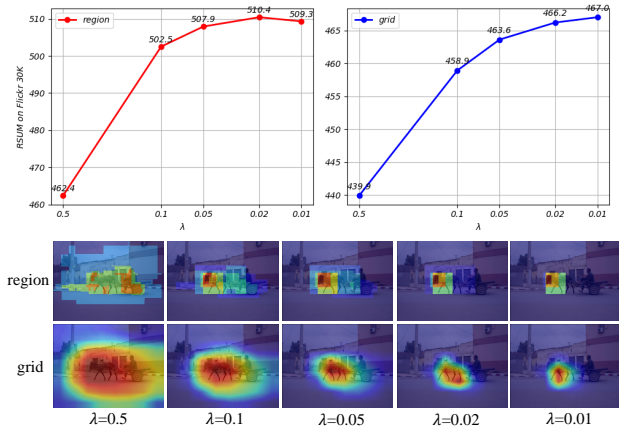


Figure 3. Upper: Performance curve on FLickr30K of hyper-parameters  $\lambda$ ; Lower: Visualized comparison between column-wise transport plans under different  $\lambda$ .

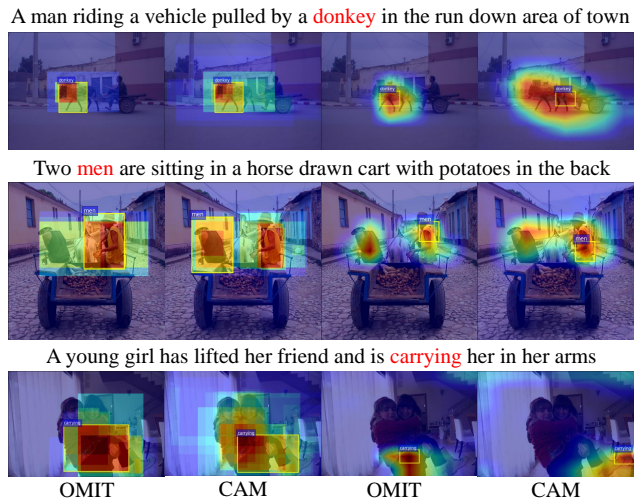


Figure 4. Visual comparisons of alignments between Our OMIT and CAM.

"donkey" and other visual fragments to the overall similarity. Remarkably, as  $\lambda$  decreases, the activated areas become smaller, indicating that "donkey" is correlated with only a minimal amount of granular visual information necessary for establishing its semantic association. This observation supports the inherent sparsity of the optimal plan, as previously highlighted in [41]. It also aligns with previous findings in [53], which suggest that a word is typically associated with a limited number of visual fragments, while the remaining fragments are redundant.

**Analysis of the Partial Matching.** We conduct ablation experiments to evaluate the effectiveness of partial matching in OMIT, as summarized in Table 4. For clarity of comparison, we present two additional partial matching variants:

Table 4. Comparisons between the baselines (CAM and naïve OT) and their corresponding improved versions using partial matching (+ Partial) on the Flickr30K test set.

TYPE	IMG → TEXT			TEXT → IMG			RSUM↑
	R@1	R@5	R@10	R@1	R@5	R@10	
<b>ResNet-152 [19] + BiGRU [13]</b>							
CAM	64.9	88.5	94.5	50.1	78.7	86.1	462.8
Partial CAM	67.4	91.1	95.3	50.5	78.5	86.8	469.7
naïve OT	66.4	89.6	94.1	51.9	79.3	86.6	468.0
Full	65.5	89.2	94.0	51.9	79.1	86.5	466.2
Prompt	66.7	89.4	93.6	51.0	78.7	86.2	465.5
Partial OT	67.6	90.6	95.2	52.5	79.3	86.6	<b>471.8</b>
<b>BUTD [2] + BiGRU [13]</b>							
CAM	79.1	95.0	97.1	58.0	84.1	90.2	503.4
Partial CAM	80.5	95.3	97.7	58.7	84.2	90.3	506.8
naïve OT	79.4	95.6	97.8	60.9	85.5	90.7	509.9
Full	79.0	95.1	98.1	61.1	85.5	91.0	509.9
Prompt	79.5	95.0	98.5	61.2	85.1	90.7	510.0
Partial OT	82.0	95.0	97.8	62.2	86.2	91.3	<b>514.5</b>

- "Full": This approach involves directly incorporating global features for full matching.
- "Prompt": Motivated by the prompt learning mechanism [7, 55], we explore the utilization of two learnable dustbins for partial matching.

Surprisingly, partial matching is not only effective for OT but also beneficial for other discrete matching methods like CAM, demonstrating the necessity of reducing redundancy. Compared to the CAM and naïve OT baselines, partial matching achieves better performance for both region and grid features, illustrating its robustness across different feature types. Compared to the naïve OT approach, the direct addition of global features for matching does not yield noticeable improvements, as it fails to provide additional information. However, the performance of the prompt-based dustbins is not significantly superior, which could be attributed to the absence of clear supervisory signals for effectively learning an optimal threshold. In our experiments, only the partial matching method demonstrates consistently favorable results. Furthermore, improvements are observed in both text retrieval and image retrieval, further demonstrating the effectiveness of partial matching in eliminating redundant alignments.

**Compared With Different Margin Initialization Strategies.** In light of the observed disparity in marginal conditions between  $\mathcal{S}_{CAM}$  and  $\mathcal{S}_{OT}$ , we delve into the performance analysis of OMIT under various margin initialization strategies. We consider four different types of margins motivated by current literature: "Uni" [38], "Intra" [31], "Inter" [56] and "Norm" [51]. In our main text, we have already adopted

the uniform margins denoted as "Uni". Here, we provide a brief explanation of each type of margin initialization:

- "Uni": Uniform margins.
- "Intra": Margins initialized based on the proximity of each fragment embedding to their respective intra-modal global embedding.
- "Inter": Margins initialized based on the proximity of each fragment embedding to their inter-modal global embedding.
- "Norm": Margins initialized based on the relative normalization value of the embeddings.

Mathematically, these margins are defined as follows:

$$\begin{aligned}
 \text{Uni: } \alpha_i &= \frac{1}{K_m}, \beta_j = \frac{1}{L_n} \\
 \text{Intra: } \alpha_i &= \frac{\exp(\bar{\mathbf{v}}^\top \mathbf{v}_i / \tau)}{\sum_i^{K_m} \exp(\bar{\mathbf{v}}^\top \mathbf{v}_i / \tau)}, \beta_j = \frac{\exp(\bar{\mathbf{t}}^\top \mathbf{t}_j / \tau)}{\sum_j^{L_n} \exp(\bar{\mathbf{t}}^\top \mathbf{t}_j / \tau)} \\
 \text{Inter: } \alpha_i &= \frac{\exp(\bar{\mathbf{t}}^\top \mathbf{v}_i / \tau)}{\sum_i^{K_m} \exp(\bar{\mathbf{t}}^\top \mathbf{v}_i / \tau)}, \beta_j = \frac{\exp(\bar{\mathbf{v}}^\top \mathbf{t}_j / \tau)}{\sum_j^{L_n} \exp(\bar{\mathbf{v}}^\top \mathbf{t}_j / \tau)} \\
 \text{Norm: } \alpha_i &= \frac{\|\tilde{\mathbf{v}}_i\|_2}{\sum_i^{K_m} \|\tilde{\mathbf{v}}_i\|_2}, \beta_j = \frac{\|\tilde{\mathbf{t}}_j\|_2}{\sum_j^{L_n} \|\tilde{\mathbf{t}}_j\|_2} \quad (7)
 \end{aligned}$$

Here,  $\mathbf{v}_i$  and  $\mathbf{t}_j$  denote one of the fragment embeddings.  $\tilde{\mathbf{v}}_i$  and  $\tilde{\mathbf{t}}_j$  are fragment embeddings before length normalization, they satisfy  $\mathbf{v}_i = \frac{\tilde{\mathbf{v}}_i}{\|\tilde{\mathbf{v}}_i\|}$  and  $\mathbf{t}_j = \frac{\tilde{\mathbf{t}}_j}{\|\tilde{\mathbf{t}}_j\|}$ .  $\tau$  is the temperature parameter. Based on empirical observations, we set  $\tau = 1$  in Equation 7 since we have found that using a smaller value for  $\tau$  leads to degraded performance.

The results in Table B1 indicate that the choice of different marginal types has limited impact on the performance of the Cross-modal Mover's Distance (CMD), highlighting its robustness within certain limits. Specifically, among the various marginal types examined, the "Intra" variant consistently performs the worst in both benchmarks. This observation suggests that relying solely on the relative proximity within a modality is an unreliable approach for calculating CMD. Conversely, the uniform margins exhibit competitive performance compared to the "Inter" and "Norm" variants. We attribute this success to the assumption of equal contributions from intra-modal fragments, which serves as a significant prior in CMD.

#### 4.4. Visualization

Figure 5-6 provides some visualizations to help understand the optimal transport plan. We visualize two row-wise alignments, which depict the relationships between a word and all regions, as well as two column-wise alignments, illustrating the connections between a region and all words. The visualizations clearly demonstrate that each word or region selectively corresponds to a sparse set of meaningful regions or words, while disregarding irrelevant candidates. Notably,

*Query: A man riding a vehicle pulled by a donkey in the run down area of town.*

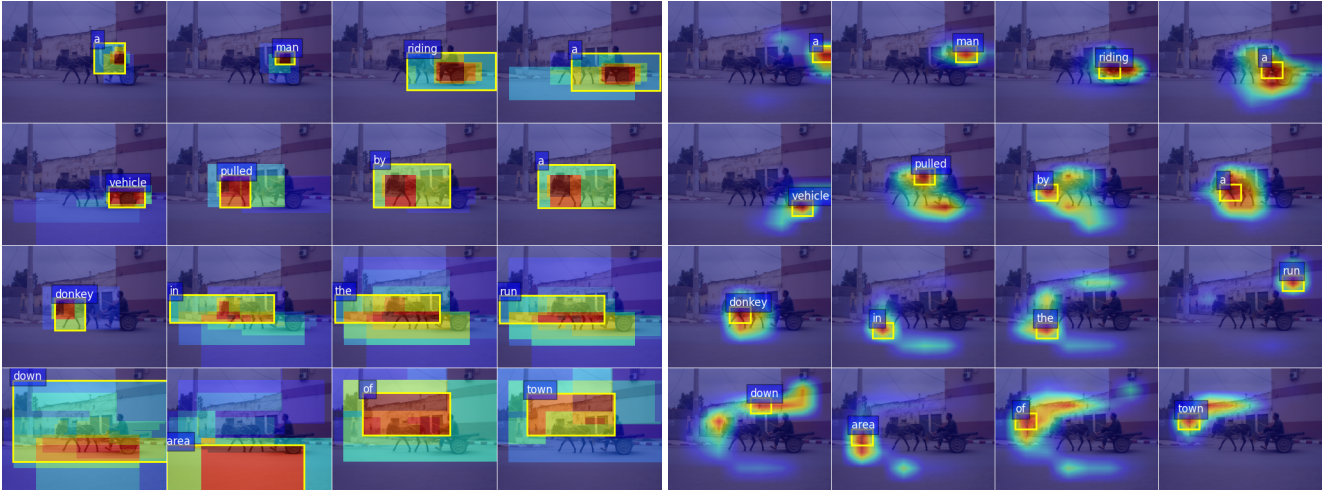


Figure 5. An illustrative example of image-text matching showcasing the column-wise transport plan generated by our OMIT variants. Left: region-based, Right: grid-based.

TYPE	IMG → TEXT			TEXT → IMG			RSUM↑
	R@1	R@5	R@10	R@1	R@5	R@10	
<b>ResNet-152 [19] + BiGRU [13]</b>							
Uni	67.0	90.3	95.6	51.8	79.4	87.1	<b>471.2</b>
Intra	65.4	88.6	93.9	51.5	78.6	86.2	464.3
Inter	67.7	89.3	94.8	51.9	79.5	86.9	470.1
Norm	68.2	88.8	94.2	52.2	79.8	87.4	470.6
<b>BUTD[2] + BiGRU [13]</b>							
Uni	78.8	95.4	98.0	60.6	85.1	91.1	509.0
Intra	78.3	95.4	97.8	59.7	85.1	90.8	507.1
Inter	78.9	95.4	98.3	59.9	84.8	91.0	508.3
Norm	80.0	95.9	97.4	59.6	85.2	91.0	<b>509.1</b>

Table 5. Comparisons of OMIT variants with different marginal conditions on the Flickr30K test set.

the words "donkey" and "vehicle" exhibit strong associations with consistent regions, and the regions representing donkey and vehicle also align well with the words "donkey," "vehicle," and their associated prefix words. These visualizations provide valuable insights into the alignment patterns of optimal transport plan that capture meaningful associations while disregarding irrelevant information.

## 5. Conclusion

In this work, we present crOss-Modal sInkhorn maTching (OMIT), which aligns fine-grained visual and semantic fragments by leveraging Optimal Transport. OMIT offers several advantages over existing matching methods. Firstly, OMIT capitalizes on granular information and explicitly es-

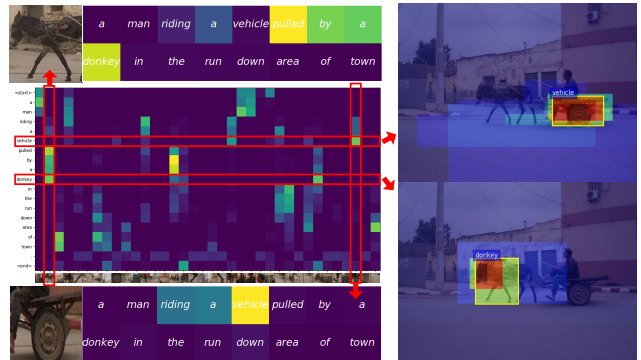


Figure 6. The visualized optimal transport plan with its row-wise and column-wise visualizations.

tablishes associations between cross-modal fragments, leading to superior performance compared to VSE and PEM. Secondly, by utilizing the Sinkhorn distance as the similarity metric, OMIT surpasses the performance of current SOTAs due to its inherent focal matching. Thirdly, OMIT bridges the efficiency gap between global embedding methods and current local matching approaches thanks to efficient Bregman iterations. By incorporating the technique of partial matching, OMIT, achieving the best results on benchmarks, demonstrating its potential. We foresee that future research in fine-grained cross-modal pre-training can be built upon the foundations established by OMIT.

## A1. Supplements to the Method

### A1.1. Revisiting Current Methods

The underlying principle of cross-modal matching revolves around associating each individual data sample, such as an image or a sentence, with a distribution in a shared space. Within this shared space, diverse semantics are demarcated by distinct regions of the distribution, effectively capturing semantic variations. One approach to construct such a distribution involves considering partial semantics as sampling points. This results in a discrete distribution that encapsulates the essence of data sample. To illustrate, consider an image denoted as  $\mathcal{V}_m = \{\mathbf{v}_i\}_{i=1}^{K_m}$  and a caption as  $\mathcal{T}_n = \{\mathbf{t}_j\}_{j=1}^{L_n}$ . Here,  $m$  and  $n$  index the dataset,  $\mathbf{v}_i \in \mathbb{R}^d$  and  $\mathbf{t}_j \in \mathbb{R}^d$  denote the image sub-regions/patches or text tokens, and  $K_m$  and  $L_n$  signify the number of fragments. The formulation of the discrete distribution  $\mathcal{V}_m$  and  $\mathcal{T}_n$  is as follows:

$$p(\mathcal{V}_m) := \sum_{i=1}^{K_m} \alpha_i \delta_{\mathbf{v}_i}, \quad p(\mathcal{T}_n) := \sum_{j=1}^{L_n} \beta_j \delta_{\mathbf{t}_j} \quad (8)$$

Here,  $\delta_x$  represents the Dirac function centered at location  $x$ , symbolizing a unit of mass.  $\alpha \in \mathbb{R}^{K_m}$  and  $\beta \in \mathbb{R}^{L_n}$  are discrete probability vectors that sum to 1. Typically, we set  $\alpha_i = \frac{1}{K_m}$  and  $\beta_j = \frac{1}{L_n}$ . The primary challenge in cross-modal matching lies in quantifying the similarity and effectively capturing the semantic relationship between  $p(\mathcal{V}_m)$  and  $p(\mathcal{T}_n)$ .

In the subsequent section, we present a succinct overview of the prevailing methods, specifically Visual-Semantic Embedding (VSE), Cross-Attention-based Method (CAM), and Probabilistic Embedding Method (PEM). This comprehensive analysis endeavors to provide a panoramic understanding and further insights.

**VSE.** The VSE methodology, while straightforward, inadvertently overlooks the high-order statistics of  $p(\mathcal{V}_m)$  and  $p(\mathcal{T}_n)$ . Rather than considering these statistics, it relies solely on the cosine similarity between the average vectors of discrete distributions to estimate their similarity. However, this approach’s limitation becomes apparent in its failure to account for high-order statistics, resulting in a lack of semantic diversity and limited effectiveness in handling ambiguity. Given that fragment embeddings are typically normalized to the unit sphere, VSE essentially computes the average

cosine similarity across all pairs of cross-modal fragments:

$$\begin{aligned} \mathcal{S}_{VSE} &:= \frac{(\frac{1}{K_m} \sum_{i=1}^{K_m} \mathbf{v}_i)^\top (\frac{1}{L_n} \sum_{j=1}^{L_n} \mathbf{t}_j)}{\|\frac{1}{K_m} \sum_{i=1}^{K_m} \mathbf{v}_i\|_2 \cdot \|\frac{1}{L_n} \sum_{j=1}^{L_n} \mathbf{t}_j\|_2} \\ &= \frac{\frac{1}{K_m L_n} \sum_{i=1}^{K_m} \sum_{j=1}^{L_n} \mathbf{v}_i^\top \mathbf{t}_j}{\|\bar{\mathbf{v}}\|_2 \cdot \|\bar{\mathbf{t}}\|_2} \\ &\stackrel{\textcircled{1}}{\geq} \sum_{i=1}^{K_m} \sum_{j=1}^{L_n} \frac{1}{K_m L_n} \mathbf{v}_i^\top \mathbf{t}_j \end{aligned} \quad (9)$$

In the above equation, the terms  $\bar{\mathbf{v}} = \frac{1}{K_m} \sum_{i=1}^{K_m} \mathbf{v}_i$  and  $\bar{\mathbf{t}} = \frac{1}{L_n} \sum_{j=1}^{L_n} \mathbf{t}_j$  represent the average (or global) embedding of  $\mathcal{V}_m$  and  $\mathcal{T}_n$ , respectively. The validity of  $\textcircled{1}$  can be attributed to the triangle inequality, which states that  $\|\frac{1}{K_m} \sum_{i=1}^{K_m} \mathbf{v}_i\|_2 \leq \frac{1}{K_m} \sum_{i=1}^{K_m} \|\mathbf{v}_i\|_2 = 1$ , similar to  $\|\bar{\mathbf{t}}\|_2 \leq 1$ . However, it should be noted that the uniform treatment of all pairwise alignments in VSE may pose challenges, as certain alignments might contribute minimally to the overall semantic coherence.

**CAM.** CAM represents an endeavor to achieve more interpretable matching results in contrast to VSE, by leveraging an attention mechanism to focus on well-aligned correspondences. The modification introduced in CAM can be observed in Equation 10, where the average operation is replaced with a weighted summation, as illustrated below:

$$\mathcal{S}_{CAM} := \sum_{i=1}^{K_m} \sum_{j=1}^{L_n} \omega_{ij} \cdot \mathbf{v}_i^\top \mathbf{t}_j \quad (10)$$

where  $\omega_{ij}$  signifies the significance of the alignment  $\mathbf{v}_i^\top \mathbf{t}_j$ , which usually obeys:

$$\begin{aligned} \omega_{ij} &:= \frac{\eta_{ij}}{\|\sum_{i=1}^{K_m} \eta_{ij} \mathbf{v}_i\|_2} \stackrel{\textcircled{2}}{\geq} \eta_{ij} \\ \text{where } \eta_{ij} &= \frac{1}{L_n} \frac{\exp(\mathbf{v}_i^\top \mathbf{t}_j / \tau)}{\sum_{i=1}^{K_m} \exp(\mathbf{v}_i^\top \mathbf{t}_j / \tau)} \end{aligned} \quad (11)$$

Here, the temperature parameter  $\tau$  is incorporated into the softmax function, as outlined by [20].  $\textcircled{2}$  holds true also due to the triangle inequality. Notably, several works [27, 36, 53] have empirically discovered that selectively disregarding certain alignments can enhance the discriminative power of  $\mathcal{S}_{CAM}$ . This observation is realized through the following equation:

$$\begin{aligned} \eta_{ij} &= \frac{1}{L_n} \frac{\exp(\mathbf{v}_i^\top \mathbf{t}_j / \tau)}{\sum_{\mathbf{v}_k \in \Delta} \exp(\mathbf{v}_k^\top \mathbf{t}_j / \tau)} \\ \text{where } \Delta &= \{\mathbf{v}_k | \mathbf{v}_k^\top \mathbf{t}_j \geq \epsilon, \forall k \in [1, K_m]\} \end{aligned} \quad (12)$$

In the above equation, the sparse threshold  $\epsilon$  varies depending on the specific methods employed.

The CAM methodology bestows greater gradient emphasis upon visual fragments that are distanced from the corresponding text tokens. This results in a more discerning representation when juxtaposed with VSE. However, CAM faces a distinct challenge of redundant alignments, which diminishes its overall effectiveness. Another noteworthy aspect is the asymmetry of  $\omega_{ij}$  in t2i (text-to-image) attention and i2t (image-to-text) attention, a characteristic present in the original CAM formulation [27]. This asymmetry introduces complexities when attempting to transfer the CAM framework to other tasks.

**PEM.** PEM considers both first-order and second-order statistics. It model the covariance of fragment embeddings and describe the data holistically using parametric Gaussian distributions. These methods utilize commonly used metrics such as  $KL$ -divergence,  $JS$ -divergence, and Wasserstein distance quantify the dissimilarity between continuous distributions. Assuming  $p(\mathcal{V}_m) \sim \mathcal{N}(\boldsymbol{\mu}_\mathcal{V}, \boldsymbol{\Sigma}_\mathcal{V})$  and  $p(\mathcal{T}_n) \sim \mathcal{N}(\boldsymbol{\mu}_\mathcal{T}, \boldsymbol{\Sigma}_\mathcal{T})$  where  $\mathcal{N}(\boldsymbol{\mu}, \boldsymbol{\Sigma})$  denotes an isotropic Gaussian distribution with the mean vector  $\boldsymbol{\mu}$  and covariance matrix  $\boldsymbol{\Sigma}$ , the discrepancy measured by the Wasserstein distance is shown in Equation 13:

$$\begin{aligned} \mathcal{D}_{PEM} &:= \min_{\gamma \in \Gamma(p(\mathcal{V}_m), p(\mathcal{T}_n))} \sqrt{\int \int_{(\mathbf{v}, \mathbf{t}) \sim \gamma} \|\mathbf{v} - \mathbf{t}\|_2^2 d\gamma(\mathbf{v}, \mathbf{t})} \\ &= \sqrt{\|\boldsymbol{\mu}_\mathcal{V} - \boldsymbol{\mu}_\mathcal{T}\|_2^2 + \|\boldsymbol{\Sigma}_\mathcal{V} - \boldsymbol{\Sigma}_\mathcal{T}\|_2^2} \end{aligned} \quad (13)$$

where  $\Gamma(p(\mathcal{V}_m), p(\mathcal{T}_n))$  denotes the sets of all joint distributions  $\gamma(\mathbf{v}, \mathbf{t})$  whose marginals are  $p(\mathcal{V}_m)$  and  $p(\mathcal{T}_n)$ , respectively. Intuitively,  $\gamma(\mathbf{v}, \mathbf{t})$  indicates how much ‘‘mass’’ must be transported from  $\mathbf{t}$  to  $\mathbf{v}$  in order to transform the distributions  $p(\mathcal{T}_n)$  into the distribution  $p(\mathcal{V}_m)$ . We argue that the improvement of PEM comes from the robust training by introducing uncertainty. However, the assumption of a parametric distribution may not be essential.

## A1.2. Methodology Details about Optimal Transport

In this subsection, we provide further details on the optimization of entropic regularized Optimal Transport. Recall the source problem

$$\begin{aligned} \mathcal{D}_{OT} &= \min_{\Omega \in \mathcal{U}(\boldsymbol{\alpha}, \boldsymbol{\beta})} \langle \Omega, \mathbf{C} \rangle := \sum_{i=1}^{K_m} \sum_{j=1}^{L_n} \omega_{ij} c_{ij} \\ \text{subject to } &\Omega \mathbf{1}_{L_n} = \boldsymbol{\alpha}, \Omega^\top \mathbf{1}_{K_m} = \boldsymbol{\beta}, \Omega \in \mathbb{R}_+^{K_m \times L_n} \end{aligned} \quad (14)$$

and its entropic regularized version:

$$\begin{aligned} \mathcal{D}_S &= \min_{\Omega \in \mathcal{U}(\boldsymbol{\alpha}, \boldsymbol{\beta})} \langle \Omega, \mathbf{C} \rangle - \lambda h(\Omega) \\ &:= \sum_{i=1}^{K_m} \sum_{j=1}^{L_n} \omega_{ij} c_{ij} + \lambda \omega_{ij} (\log \omega_{ij} - 1) \end{aligned} \quad (15)$$

where  $h(\Omega) = -\sum_{i=1}^{K_m} \sum_{j=1}^{L_n} \omega_{ij} (\log \omega_{ij} - 1)$  is the entropic term;  $\omega_{ij}$  and  $c_{ij}$  refer to the element in the  $i$ -th row and  $j$ -th column of the plan matrix  $\Omega$  and cost matrix  $\mathbf{C}$ , respectively. By introducing entropic regularization, the source problem is transformed into a  $p$ -strongly convex problem, which can be efficiently solved using Lagrange multipliers:

$$\begin{aligned} \mathcal{J}(\Omega, \boldsymbol{\mu}, \boldsymbol{\theta}) &= \langle \Omega, \mathbf{C} \rangle - \lambda h(\Omega) \\ &- \boldsymbol{\mu}^\top (\Omega \mathbf{1}_{L_n} - \boldsymbol{\alpha}) - \boldsymbol{\theta}^\top (\Omega^\top \mathbf{1}_{K_m} - \boldsymbol{\beta}) \end{aligned} \quad (16)$$

where  $\boldsymbol{\mu} \in \mathbb{R}^{K_m}, \boldsymbol{\theta} \in \mathbb{R}^{L_m}$  are the dual variables for the two equality constraints in  $\mathcal{U}(\boldsymbol{\alpha}, \boldsymbol{\beta})$ . For any couple  $(i, j)$ , When  $\frac{\partial \mathcal{J}}{\partial \omega_{ij}} = c_{ij} + \lambda \log(\omega_{ij}) - \mu_i - \theta_j = 0$ , Equation 15 obtains the unique solution  $\Omega^*$  whose every element obeys the form  $\omega_{ij} = e^{\frac{\mu_i}{\lambda}} e^{-\frac{c_{ij}}{\lambda}} e^{\frac{\theta_j}{\lambda}}$ . To this end,  $\Omega^*$  has the form:

$$\Omega^* = \text{diag}(\boldsymbol{\mu}^{(t)}) \boldsymbol{\xi} \text{diag}(\boldsymbol{\theta}^{(t)}) \quad (17)$$

where  $\boldsymbol{\xi} = e^{-\frac{\mathbf{C}}{\lambda}}$  is the Gibbs kernel as previously stated in the main text,  $\boldsymbol{\mu}^{(t)}$  and  $\boldsymbol{\theta}^{(t)}$  are the projected vector to be calculated, which can be obtained by transforming  $\boldsymbol{\mu}$  and  $\boldsymbol{\theta}$ . Directly seeking the analytical solutions of  $\boldsymbol{\mu}$  and  $\boldsymbol{\theta}$  can be complicated; hence, iterative optimization is a better approach. According to [38], current optimization solutions of Equation 15 are mainly from two perspectives, namely matrix scaling [14] and alternating projection [4]. Both are essentially equivalent, and we adopt the latter method in our main text.

**Matrix scaling.** Specifically, to satisfy the marginal condition of  $\Omega^*$ , we combine it with Equation 17, leading to the following expression:

$$\boldsymbol{\mu}^{(t)} \odot (\boldsymbol{\xi} \boldsymbol{\theta}^{(t)}) = \boldsymbol{\alpha}, \quad \boldsymbol{\theta}^{(t)} \odot (\boldsymbol{\xi}^\top \boldsymbol{\mu}^{(t)}) = \boldsymbol{\beta} \quad (18)$$

where  $\odot$  refers to the Hadamard product. The problem of solving Equation 18, which involves scaling the rows and columns of the matrix  $\mathbf{K}$  to satisfy the given marginal constraints, is widely known in the numerical analysis community as the matrix scaling problem [35]. This problem can be efficiently solved using the well-known Sinkhorn-Knopp algorithm [24], which can be expressed as:

$$\boldsymbol{\mu}^{(t+1)} = \frac{\boldsymbol{\alpha}}{\boldsymbol{\xi} \boldsymbol{\theta}^{(t)}}, \quad \boldsymbol{\theta}^{(t+1)} = \frac{\boldsymbol{\beta}}{\boldsymbol{\xi}^\top \boldsymbol{\mu}^{(t+1)}} \quad (19)$$

The division operator here denotes the Hadamard division. The convergence proof of Equation 19 is attributed to Sinkhorn and Knopp [42], hence the name of the algorithm. The initiation of  $\boldsymbol{\theta}^{(0)}$  can be arbitrary, such as  $\boldsymbol{\theta}^{(0)} = \mathbf{1}_{L_n}$ .

**Alternating projection.** Equation 15 can be re-cast as fol-

Caption: A man riding a vehicle pulled by a **donkey** in the run down area of town.

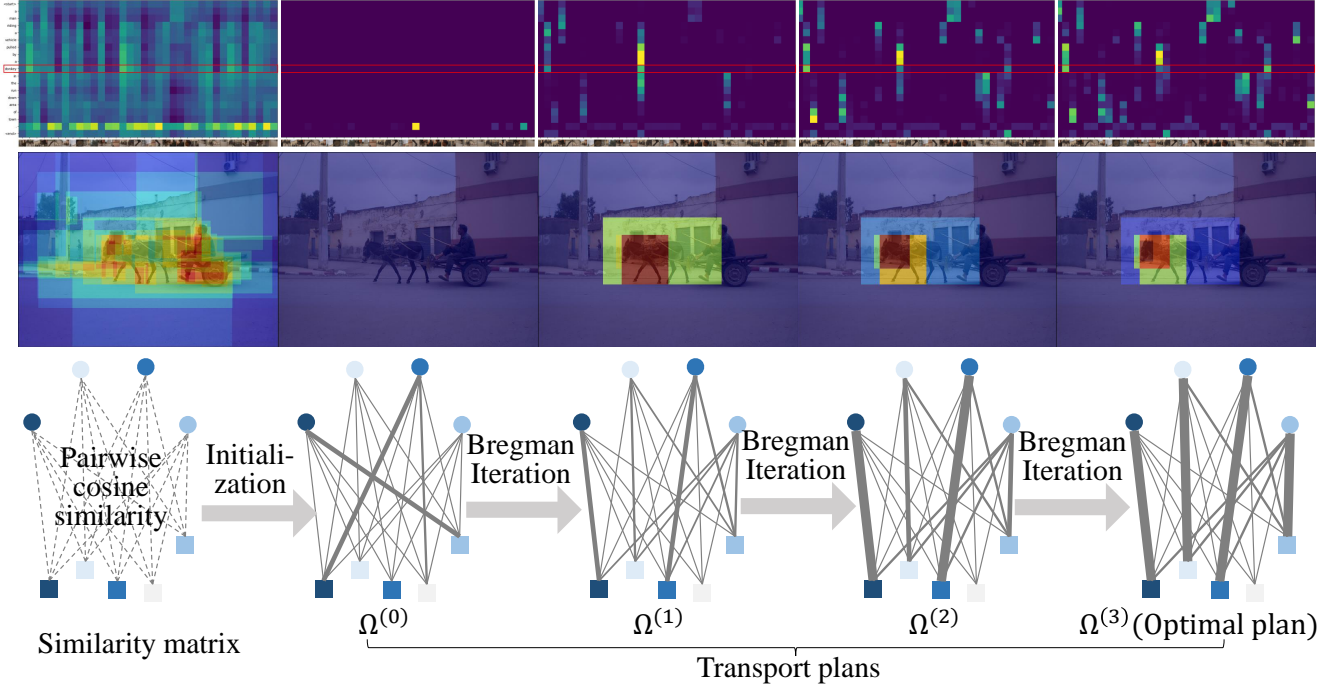


Figure A1. An illustration of the Sinkhorn matching module which is elaborated in the main text. Each column corresponds to a time step, and the three rows from top to bottom respectively depict the changes over iterations in the overall transport plan, the row-wise transport plan and the demo sketch. It's evident that the transport plan gradually becomes sparser as the iterations process.

lows:

$$\begin{aligned}
 \mathcal{D}_S &= \min_{\Omega \in \mathcal{U}(\alpha, \beta)} \lambda \sum_{i=1}^{K_m} \sum_{j=1}^{L_n} \omega_{ij} \left( \log \frac{\omega_{ij}}{e^{-\frac{c_{ij}}{\lambda}}} - 1 \right) \\
 &= \min_{\Omega \in \mathcal{U}(\alpha, \beta)} \lambda KL(\Omega | \xi) \\
 &:= \lambda \sum_{i=1}^{K_m} \sum_{j=1}^{L_n} \left( \omega_{ij} \log \frac{\omega_{ij}}{\xi_{ij}} - \omega_{ij} + \xi_{ij} \right)
 \end{aligned} \tag{20}$$

If the convex sets  $\mathcal{U}(\alpha, \beta)$  are indeed affine subspaces, then Equation 20 can be solved simply using naïve Bregman projections:

$$\Omega^* = Proj_{\mathcal{U}(\alpha, \beta)}^{KL}(\Omega) := \underset{\Omega \in \mathcal{U}(\alpha, \beta)}{\operatorname{argmin}} KL(\Omega | \xi) \tag{21}$$

However, denoting  $\mathcal{C}_\alpha^1 := \{\Omega \in \mathbb{R}_+^{K_m \times L_n} | \Omega \mathbf{1}_{L_n} = \alpha\}$  and  $\mathcal{C}_\beta^2 := \{\Omega \in \mathbb{R}_+^{K_m \times L_n} | \Omega^\top \mathbf{1}_{K_m} = \beta\}$  the rows and columns constraints, we have  $\mathcal{U}(\alpha, \beta) = \mathcal{C}_\alpha^1 \cap \mathcal{C}_\beta^2$ . It can be shown that the convex set  $\mathcal{U}(\alpha, \beta)$  is the intersection of these two affine subspaces, i.e.,  $\mathcal{C}_\alpha^1$  and  $\mathcal{C}_\beta^2$ . Due to this non-trivial intersection, the naïve Bregman projections in Equation 21 do not converge to the optimal solution. Fortunately, as discussed in [4], this issue can be addressed by extending the Dykstra algorithm [5] to the KL setting, that

is:

$$\begin{aligned}
 \Omega^* &= \underset{\Omega \in \mathcal{C}_\alpha^1 \cap \mathcal{C}_\beta^2}{\operatorname{argmin}} KL(\Omega | \xi) \\
 &:= Proj_{\mathcal{C}_\beta^2}^{KL} \left( Proj_{\mathcal{C}_\alpha^1}^{KL}(\Omega) \right)
 \end{aligned} \tag{22}$$

According to [4], we have:

$$\begin{aligned}
 \Omega^{(2t+1)} &= Proj_{\mathcal{C}_\alpha^1}^{KL}(\Omega^{(2t)}) \\
 &:= \operatorname{diag}\left(\frac{\alpha}{\Omega^{(2t)} \mathbf{1}_{L_n}}\right) \Omega^{(2t)} \\
 \Omega^{(2t+2)} &= Proj_{\mathcal{C}_\beta^2}^{KL}(\Omega^{(2t+1)})
 \end{aligned} \tag{23}$$

$$:= \Omega^{(2t+1)} \operatorname{diag}\left(\frac{\beta}{\Omega^{(2t+1)\top} \mathbf{1}_{K_m}}\right)$$

Initialize  $\Omega^{(0)} = \xi$

To this end, We provide the derivation of solving the entropic regularized Optimal Transport by alternating Bregman projections. Algorithm A1 provides an overview of the Bregman iterations for image-text matching. Notably, iterations behind Equation 19 can be viewed as a special case of iterations behind Equation 23, as demonstrated in [38]. In our main text, we adopt Equation 23 to optimize the sinkhorn distance for which we can directly visualize the intermediate transport plan  $\Omega^{(2t)}$  of each  $t$ .

---

**Algorithm A1** Leveraging Bregman iterations to optimize the Sinkhorn distance between an image and a caption.

---

**Input:** Fragment embeddings of an image  $\mathcal{V}_m \in \mathbb{R}^{K_m \times d}$ , fragment embeddings of a caption  $\mathcal{T}_n \in \mathbb{R}^{L_n \times d}$ , hyperparameter  $\lambda$ .

**Output:** Sinkhorn similarity  $\mathcal{S}_{OT}$ .

- 1: Calculate the cost matrix:  $\mathbf{C} = 1 - \mathcal{V}_m \mathcal{T}_n^\top \in \mathbb{R}^{K_m \times L_n}$ .
  - 2: Calculate the initial transport plan:  $\Omega^{(0)} = e^{-\frac{\mathbf{C}}{\lambda}}$ .
  - 3: Initialize  $\alpha = \frac{1}{K_m} \mathbf{1}_{K_m}$ ,  $\beta = \frac{1}{L_n} \mathbf{1}_{L_n}$ ,  $\varepsilon = 1e - 6$ , maximum iterations  $T = 3$ .
  - 4: **for**  $t = 1, \dots, T$  **do**
  - 5: Perform row-wise normalization:  $\Omega^{(t)} \leftarrow \text{diag}(\frac{\alpha}{\Omega^{(t)} \mathbf{1}_{L_n}}) \Omega^{(t-1)}$
  - 6: Perform column-wise normalization:  $\Omega^{(t)} \leftarrow \Omega^{(t)} \text{diag}(\frac{\beta}{\Omega^{(t)\top} \mathbf{1}_{K_m}})$
  - 7: **if**  $\|\Omega^{(t)} - \Omega^{(t-1)}\|_2 / \|\Omega^{(t-1)}\|_2 < \varepsilon$  **then**
  - 8: **break**
  - 9: **end if**
  - 10: **end for**
  - 11: Calculate the Sinkhorn similarity:  $\mathcal{S}_{OT} = 1 - \langle \Omega^{(t)}, \mathcal{V}_m \mathcal{T}_n^\top \rangle$
  - 12: **return**  $\mathcal{S}_{OT}$
- 

Furthermore, the similarity between an image  $\mathcal{V}_m$  and a caption  $\mathcal{T}_n$  using Optimal Transport, as defined in Equation 6 of our main text, can be expressed as:

$$\mathcal{S}_{OT} = \langle \Omega^*, \mathcal{V}_m \mathcal{T}_n^\top \rangle := \sum_{i=1}^{K_m} \sum_{j=1}^{L_n} \omega_{ij} \cdot \mathbf{v}_i^\top \mathbf{t}_j \quad (24)$$

$$\text{where } \sum_{j=1}^{L_n} \omega_{ij} = \alpha_i, \sum_{i=1}^{K_m} \omega_{ij} = \beta_j, \sum_{i=1}^{K_m} \sum_{j=1}^{L_n} \omega_{ij} = 1$$

Combining Equation 9, 10 and 24 we can find that  $\mathcal{S}_{OT}$  serves as an upper bound of  $\mathcal{S}_{VSE}$  and  $\mathcal{S}_{CAM}$ . However, the disparity arises from the fact that the marginal conditions of  $\omega$  in  $\mathcal{S}_{VSE}$  align with those of  $\mathcal{S}_{OT}$ , whereas the marginal conditions of  $\omega$  in  $\mathcal{S}_{CAM}$  do not align. In light of these findings, it is more reasonable to directly compare the bound similarities rather than relying solely on empirical similarities.

We present a visualization of the Bregman iterations used to solve Equation 23 in Figure A1, which specifies the Sinkhorn Matching module of Figure 2 in the main text. The upper row of Figure A1 depicts the similarity matrix (inverse cost matrix) and transport plans  $\Omega^{(t)}$  at each step  $t$  (here  $t = 0, \dots, 3$ ). The middle row shows the alignments between the word "donkey" in the caption and all other salient regions in the image, which correspond to the row in  $\Omega^{(t)}$  marked with a red box. The lower row is a sketch illus-

trating the iterations. From the first column of Figure A1, we can see that the original cost matrix is chaotic, with many irrelevant regions contributing, which partially demonstrates that simply averaging all these contributions, as done in VSE, will lead to inferior results. The initial transport plan is extremely sparse and meaningless under a small  $\lambda$ , but after row-wise and column-wise projections, the transport plan becomes diverse and meaningful. As the iterations progress,  $\Omega^{(t)}$  gradually eliminates the disturbance from meaningless regions and concentrates more on relevant regions. Eventually, all other irrelevant regions are ignored, resulting in an optimal plan that aligns the significant fragmented pairs.

## B1. Supplements to Experiments

### B1.1. More Ablation Studies

**Compared With Different Margin Initialization Strategies.** In light of the observed disparity in marginal conditions between  $\mathcal{S}_{CAM}$  and  $\mathcal{S}_{OT}$ , we delve into the performance analysis of OMIT under various margin initialization strategies. We consider four different types of margins motivated by current literature: "Uni" [38], "Intra" [31], "Inter" [56] and "Norm" [51]. In our main text, we have already adopted the uniform margins denoted as "Uni". Here, we provide a brief explanation of each type of margin initialization:

- "Uni": Uniform margins used in our main text.
- "Intra": Margins initialized based on the proximity of each fragment embedding to their respective intra-modal global embedding.
- "Inter": Margins initialized based on the proximity of each fragment embedding to their inter-modal global embedding.
- "Uni": Margins initialized based on the relative normalization value of the embeddings.

Mathematically, these margins are defined as follows:

$$\begin{aligned} \text{Uni: } \alpha_i &= \frac{1}{K_m}, \beta_j = \frac{1}{L_n} \\ \text{Intra: } \alpha_i &= \frac{\exp(\bar{\mathbf{v}}^\top \mathbf{v}_i / \tau)}{\sum_i^{K_m} \exp(\bar{\mathbf{v}}^\top \mathbf{v}_i / \tau)}, \beta_j = \frac{\exp(\bar{\mathbf{t}}^\top \mathbf{t}_j / \tau)}{\sum_j^{L_n} \exp(\bar{\mathbf{t}}^\top \mathbf{t}_j / \tau)} \\ \text{Inter: } \alpha_i &= \frac{\exp(\bar{\mathbf{t}}^\top \mathbf{v}_i / \tau)}{\sum_i^{K_m} \exp(\bar{\mathbf{t}}^\top \mathbf{v}_i / \tau)}, \beta_j = \frac{\exp(\bar{\mathbf{v}}^\top \mathbf{t}_j / \tau)}{\sum_j^{L_n} \exp(\bar{\mathbf{v}}^\top \mathbf{t}_j / \tau)} \\ \text{Norm: } \alpha_i &= \frac{\|\tilde{\mathbf{v}}_i\|_2}{\sum_i^{K_m} \|\tilde{\mathbf{v}}_i\|_2}, \beta_j = \frac{\|\tilde{\mathbf{t}}_j\|_2}{\sum_j^{L_n} \|\tilde{\mathbf{t}}_j\|_2} \quad (25) \end{aligned}$$

Here,  $\mathbf{v}_i$  and  $\mathbf{t}_j$  denote one of the fragment embeddings.  $\tilde{\mathbf{v}}_i$  and  $\tilde{\mathbf{t}}_j$  are fragment embeddings before length normalization, they satisfies  $\mathbf{v}_i = \frac{\tilde{\mathbf{v}}_i}{\|\tilde{\mathbf{v}}_i\|}$  and  $\mathbf{t}_j = \frac{\tilde{\mathbf{t}}_j}{\|\tilde{\mathbf{t}}_j\|}$ .  $\tau$  is the temperature parameter. Based on empirical observations, we set  $\tau = 1$  in Equation 25 since we have found that using a smaller value for  $\tau$  leads to degraded performance.

*Query: Two men standing on the back of a cart pulled by horses.*

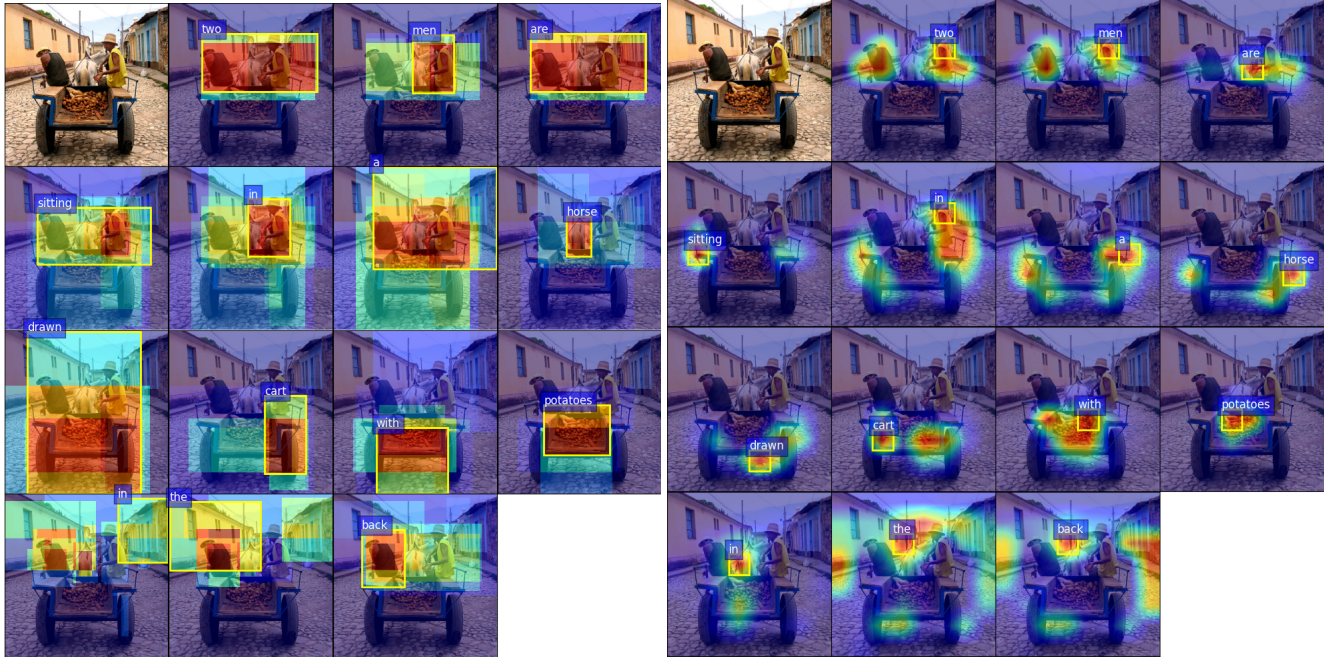


Figure B1. An illustrative example of image-text matching showcasing the column-wise transport plan generated by our OMIT variants. Left: region-based OMIT; Right: grid-based OMIT.

*Query: Two girls with one girl carrying another girl on her back.*

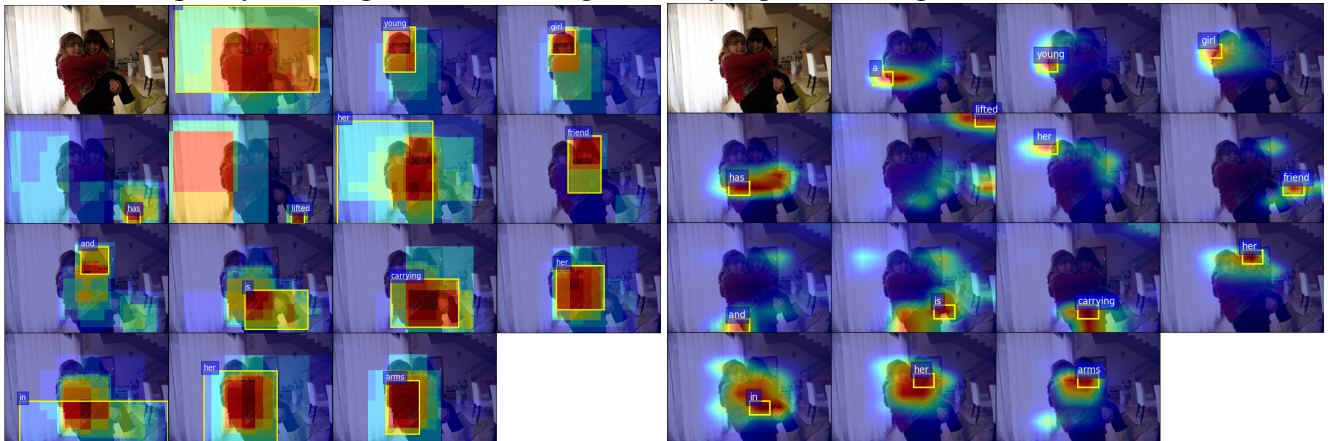


Figure B2. An illustrative example of image-text matching demonstrating the column-wise transport plan generated by our OMIT variants. Left: region-based OMIT; Right: grid-based OMIT.

The results in Table B1 indicate that the choice of different marginal types has limited impact on the performance of the Cross-modal Mover's Distance (CMD), highlighting its robustness within certain limits. Specifically, among the various marginal types examined, the "Intra" variant consistently performs the worst in both benchmarks. This observation suggests that relying solely on the relative proximity within a modality is an unreliable approach for calculating CMD.

Conversely, the uniform margins exhibit competitive performance compared to the "Inter" and "Norm" variants. We attribute this success to the assumption of equal contributions from intra-modal fragments, which serves as a significant prior in CMD.

TYPE	IMG → TEXT			TEXT → IMG			RSUM↑
	R@1	R@5	R@10	R@1	R@5	R@10	
<b>ResNet-152 [19] + BiGRU [13]</b>							
Uni	67.0	90.3	95.6	51.8	79.4	87.1	<b>471.2</b>
Intra	65.4	88.6	93.9	51.5	78.6	86.2	464.3
Inter	67.7	89.3	94.8	51.9	79.5	86.9	470.1
Norm	68.2	88.8	94.2	52.2	79.8	87.4	470.6
<b>BUTD[2] + BiGRU [13]</b>							
Uni	78.8	95.4	98.0	60.6	85.1	91.1	509.0
Intra	78.3	95.4	97.8	59.7	85.1	90.8	507.1
Inter	78.9	95.4	98.3	59.9	84.8	91.0	508.3
Norm	80.0	95.9	97.4	59.6	85.2	91.0	<b>509.1</b>

Table B1. Comparisons of OMIT variants with different marginal conditions on the Flickr30K test set.

## B1.2. More Visualizations

Figures B1-B2 illustrate the comprehensive alignments achieved by OMIT when utilizing two sets of backbones: BUTD+BiGRU and ResNet-152+BiGRU. In-depth analysis of these figures reveals that ostensive semantics, such as "vehicle," "horse," and "girl," can be effectively represented using only a few sub-regions or pixels. However, the visualization of abstract concepts, function words, and relational words like "back," "of," and "lifted" presents challenges in visual representation, leading to figures that display meaningless chunks or even provide incorrect indications. Furthermore, in Figure B1 and Figure B2, OMIT encounters difficulties in distinguishing between the two girls, incorrectly identifying the girls lifting as the girl being lifted. These observations highlight the inherent limitation of OMIT, which primarily models co-occurrences but lacks the cognitive and reasoning capabilities necessary for accurate understanding. We speculate that incorporating the high-order relations may help overcome these limitations and eagerly anticipate further exploration in this direction.

## References

- [1] Sungtae An, Nataraj Jammalamadaka, and Eunji Chong. Maximum entropy information bottleneck for uncertainty-aware stochastic embedding. In *CVPR*, pages 3808–3817, 2023. 2
- [2] Peter Anderson, Xiaodong He, Chris Buehler, Damien Teney, Mark Johnson, Stephen Gould, and Lei Zhang. Bottom-up and top-down attention for image captioning and visual question answering. In *CVPR*, pages 6077–6086, 2018. 4, 5, 7, 8, 9, 15
- [3] Martin Arjovsky, Soumith Chintala, and Léon Bottou. Wasserstein generative adversarial networks. In *International Conference on Machine Learning*, pages 214–223, 2017. 3
- [4] Jean-David Benamou, Guillaume Carlier, Marco Cuturi, Luca Nenna, and Gabriel Peyré. Iterative bregman projections for regularized transportation problems. *SIAM Journal on Scientific Computing*, 37(2):A1111–A1138, 2015. 4, 11, 12
- [5] James P Boyle and Richard L Dykstra. A method for finding projections onto the intersection of convex sets in hilbert spaces. In *Advances in Order Restricted Statistical Inference: Proceedings of the Symposium on Order Restricted Statistical Inference held in Iowa City, Iowa, September 11–13, 1985*, pages 28–47. Springer, 1986. 12
- [6] Lev M Bregman. The relaxation method of finding the common point of convex sets and its application to the solution of problems in convex programming. *USSR Computational Mathematics and Mathematical Physics*, 7(3):200–217, 1967. 3
- [7] Tom Brown, Benjamin Mann, Nick Ryder, Melanie Subbiah, Jared D Kaplan, Prafulla Dhariwal, Arvind Neelakantan, Pranav Shyam, Girish Sastry, Amanda Askell, et al. Language models are few-shot learners. *Advances in neural information processing systems*, 33:1877–1901, 2020. 8
- [8] Hui Chen, Guiguang Ding, Xudong Liu, Zijia Lin, Ji Liu, and Jungong Han. Imram: Iterative matching with recurrent attention memory for cross-modal image-text retrieval. In *CVPR*, pages 12655–12663, 2020. 2, 5
- [9] Jiacheng Chen, Hexiang Hu, Hao Wu, Yuning Jiang, and Changhu Wang. Learning the best pooling strategy for visual semantic embedding. In *CVPR*, pages 15789–15798, 2021. 2, 5, 6
- [10] Liqun Chen, Zhe Gan, Yu Cheng, Linjie Li, Lawrence Carin, and Jingjing Liu. Graph optimal transport for cross-domain alignment. In *International Conference on Machine Learning*, pages 1542–1553, 2020. 3
- [11] Xing Cheng, Hezheng Lin, Xiangyu Wu, Fan Yang, and Dong Shen. Improving video-text retrieval by multi-stream corpus alignment and dual softmax loss. *arXiv preprint arXiv:2109.04290*, 2021. 5
- [12] Sanghyuk Chun, Seong Joon Oh, Rafael Sampaio De Rezende, Yannis Kalantidis, and Diane Larlus. Probabilistic embeddings for cross-modal retrieval. In *CVPR*, pages 8415–8424, 2021. 2, 5
- [13] Junyoung Chung, Caglar Gulcehre, KyungHyun Cho, and Yoshua Bengio. Empirical evaluation of gated recurrent neural networks on sequence modeling. *arXiv preprint arXiv:1412.3555*, 2014. 4, 5, 7, 8, 9, 15
- [14] Marco Cuturi. Sinkhorn distances: lightspeed computation of optimal transport. In *Advances in Neural Information Processing Systems*, pages 2292–2300, 2013. 2, 4, 11
- [15] Haiwen Diao, Ying Zhang, Lin Ma, and Huchuan Lu. Similarity reasoning and filtration for image-text matching. In *Proceedings of the AAAI Conference on Artificial Intelligence*, pages 1218–1226, 2021. 5
- [16] Fartash Faghri, David J Fleet, Jamie Ryan Kiros, and Sanja Fidler. Vse++: Improving visual-semantic embeddings with hard negatives. *arXiv preprint arXiv:1707.05612*, 2017. 2, 5, 6
- [17] Andrea Frome, Greg S Corrado, Jon Shlens, Samy Bengio, Jeff Dean, Marc’Aurelio Ranzato, and Tomas Mikolov. Devise: A deep visual-semantic embedding model. In *Advances in Neural Information Processing Systems*, pages 4357–3469, 2013. 1, 2
- [18] Zheren Fu, Zhendong Mao, Yan Song, and Yongdong Zhang. Learning semantic relationship among instances for image-text matching. In *CVPR*, pages 15159–15168, 2023. 5
- [19] Kaiming He, Xiangyu Zhang, Shaoqing Ren, and Jian Sun. Deep residual learning for image recognition. In *CVPR*, pages 770–778, 2016. 4, 5, 7, 8, 9, 15
- [20] Geoffrey Hinton, Oriol Vinyals, and Jeff Dean. Distilling the knowledge in a neural network. *arXiv preprint arXiv:1503.02531*, 2015. 10
- [21] Huaizu Jiang, Ishan Misra, Marcus Rohrbach, Erik Learned-Miller, and Xinlei Chen. In defense of grid features for visual question answering. In *CVPR*, pages 10267–10276, 2020. 4
- [22] Jacob Devlin Ming-Wei Chang Kenton and Lee Kristina Toutanova. Bert: Pre-training of deep bidirectional transformers for language understanding. In *Proceedings of the North American Chapter of the Association for Computational Linguistics*, pages 4171–4186, 2019. 4, 5
- [23] Dongwon Kim, Namyup Kim, and Suha Kwak. Improving cross-modal retrieval with set of diverse embeddings. In *CVPR*, pages 23422–23431, 2023. 5
- [24] Philip A Knight. The sinkhorn–knopp algorithm: convergence and applications. *SIAM Journal on Matrix Analysis and Applications*, 30(1):261–275, 2008. 11
- [25] Ranjay Krishna, Yuke Zhu, Oliver Groth, Justin Johnson, Kenji Hata, Joshua Kravitz, Stephanie Chen, Yannis Kalantidis, Li-Jia Li, David A Shamma, et al. Visual genome: Connecting language and vision using crowdsourced dense image annotations. *International Journal of Computer Vision*, 123:32–73, 2017. 4
- [26] Matt Kusner, Yu Sun, Nicholas Kolkin, and Kilian Weinberger. From word embeddings to document distances. In *International Conference on Machine Learning*, pages 957–966, 2015. 3
- [27] Kuang-Huei Lee, Xi Chen, Gang Hua, Houdong Hu, and Xiaodong He. Stacked cross attention for image-text matching. In *Proceedings of the European Conference on Computer Vision*, pages 201–216, 2018. 1, 5, 10, 11
- [28] Kunpeng Li, Yulun Zhang, Kai Li, Yuanyuan Li, and Yun Fu. Visual semantic reasoning for image-text matching. In *Proceedings of the IEEE International Conference on Computer Vision*, pages 4654–4662, 2019. 2, 5

- [29] Kunpeng Li, Yulun Zhang, Kai Li, Yuanyuan Li, and Yun Fu. Image-text embedding learning via visual and textual semantic reasoning. *IEEE Transactions on Pattern Analysis and Machine Intelligence*, 45(1):641–656, 2022. 5
- [30] Tsung-Yi Lin, Michael Maire, Serge Belongie, James Hays, Pietro Perona, Deva Ramanan, Piotr Dollár, and C Lawrence Zitnick. Microsoft coco: Common objects in context. In *Proceedings of the European Conference on Computer Vision*, pages 740–755, 2014. 2, 5, 6
- [31] Chunxiao Liu, Zhendong Mao, An-An Liu, Tianzhu Zhang, Bin Wang, and Yongdong Zhang. Focus your attention: A bidirectional focal attention network for image-text matching. In *Proceedings of the 27th ACM international conference on multimedia*, pages 3–11, 2019. 8, 13
- [32] Ilya Loshchilov and Frank Hutter. Decoupled weight decay regularization. *arXiv preprint arXiv:1711.05101*, 2017. 6
- [33] Dhruv Mahajan, Ross Girshick, Vignesh Ramanathan, Kaiming He, Manohar Paluri, Yixuan Li, Ashwin Bharambe, and Laurens Van Der Maaten. Exploring the limits of weakly supervised pretraining. In *Proceedings of the European Conference on Computer Vision*, pages 181–196, 2018. 5
- [34] Nicola Messina, Giuseppe Amato, Andrea Esuli, Fabrizio Falchi, Claudio Gennaro, and Stéphane Marchand-Maillet. Fine-grained visual textual alignment for cross-modal retrieval using transformer encoders. *ACM Transactions on Multimedia Computing, Communications, and Applications (TOMM)*, 17(4):1–23, 2021. 5
- [35] Arkadi Nemirovski and Uriel Rothblum. On complexity of matrix scaling. *Linear Algebra and its Applications*, 302: 435–460, 1999. 11
- [36] Zhengxin Pan, Fangyu Wu, and Bailing Zhang. Fine-grained image-text matching by cross-modal hard aligning network. In *CVPR*, pages 19275–19284, 2023. 2, 3, 5, 10
- [37] Jeffrey Pennington, Richard Socher, and Christopher D Manning. Glove: Global vectors for word representation. In *EMNLP*, pages 1532–1543, 2014. 4
- [38] Gabriel Peyré, Marco Cuturi, et al. Computational optimal transport: With applications to data science. *Foundations and Trends® in Machine Learning*, 11(5-6):355–607, 2019. 3, 8, 11, 12, 13
- [39] Alec Radford, Jong Wook Kim, Chris Hallacy, Aditya Ramesh, Gabriel Goh, Sandhini Agarwal, Girish Sastry, Amanda Askell, Pamela Mishkin, Jack Clark, et al. Learning transferable visual models from natural language supervision. In *International conference on machine learning*, pages 8748–8763. PMLR, 2021. 5
- [40] Shaoqing Ren, Kaiming He, Ross Girshick, and Jian Sun. Faster r-cnn: Towards real-time object detection with region proposal networks. *IEEE Transactions on Pattern Analysis and Machine Intelligence*, 39(06):1137–1149, 2017. 4
- [41] Yossi Rubner, Carlo Tomasi, and Leonidas J Guibas. The earth mover’s distance as a metric for image retrieval. *International Journal of Computer Vision*, 40(2):99, 2000. 3, 7
- [42] Richard Sinkhorn. A relationship between arbitrary positive matrices and doubly stochastic matrices. *The annals of mathematical statistics*, 35(2):876–879, 1964. 11
- [43] Yale Song and Mohammad Soleymani. Polysemous visual-semantic embedding for cross-modal retrieval. In *CVPR*, pages 1979–1988, 2019. 1, 5
- [44] Haoran Wang, Ying Zhang, Zhong Ji, Yanwei Pang, and Lin Ma. Consensus-aware visual-semantic embedding for image-text matching. In *Proceedings of the European Conference on Computer Vision*, pages 18–34, 2020. 2
- [45] Yun Wang, Tong Zhang, Xueya Zhang, Zhen Cui, Yuge Huang, Pengcheng Shen, Shaoxin Li, and Jian Yang. Wasserstein coupled graph learning for cross-modal retrieval. In *Proceedings of the IEEE International Conference on Computer Vision*, pages 1793–1802. IEEE, 2021. 3
- [46] Zheng Wang, Zhenwei Gao, Kangshuai Guo, Yang Yang, Xiaoming Wang, and Heng Tao Shen. Multilateral semantic relations modeling for image text retrieval. In *CVPR*, pages 2830–2839, 2023. 2
- [47] Jiwei Wei, Yang Yang, Xing Xu, Xiaofeng Zhu, and Heng Tao Shen. Universal weighting metric learning for cross-modal retrieval. *IEEE Transactions on Pattern Analysis and Machine Intelligence*, 44(10):6534–6545, 2021. 6
- [48] Xi Wei, Tianzhu Zhang, Yan Li, Yongdong Zhang, and Feng Wu. Multi-modality cross attention network for image and sentence matching. In *Proceedings of the IEEE/CVF conference on computer vision and pattern recognition*, pages 10941–10950, 2020. 5
- [49] Saining Xie, Ross Girshick, Piotr Dollár, Zhuowen Tu, and Kaiming He. Aggregated residual transformations for deep neural networks. In *CVPR*, pages 1492–1500, 2017. 4
- [50] Jinyu Yang, Jiali Duan, Son Tran, Yi Xu, Sampath Chanda, Liqun Chen, Belinda Zeng, Trishul Chilimbi, and Junzhou Huang. Vision-language pre-training with triple contrastive learning. In *CVPR*, pages 15671–15680, 2022. 4
- [51] Sho Yokoi, Ryo Takahashi, Reina Akama, Jun Suzuki, and Kentaro Inui. Word rotator’s distance: Decomposing vectors gives better representations. *arXiv preprint arXiv:2004.15003*, 2020. 8, 13
- [52] Peter Young, Alice Lai, Micah Hodosh, and Julia Hockenmaier. From image descriptions to visual denotations: New similarity metrics for semantic inference over event descriptions. *Transactions of the Association for Computational Linguistics*, 2:67–78, 2014. 2, 5, 6
- [53] Kun Zhang, Zhendong Mao, Quan Wang, and Yongdong Zhang. Negative-aware attention framework for image-text matching. In *CVPR*, pages 15661–15670, 2022. 2, 3, 5, 7, 10
- [54] Qi Zhang, Zhen Lei, Zhaoxiang Zhang, and Stan Z Li. Context-aware attention network for image-text retrieval. In *Proceedings of the IEEE/CVF conference on computer vision and pattern recognition*, pages 3536–3545, 2020. 5
- [55] Kaiyang Zhou, Jingkang Yang, Chen Change Loy, and Ziwei Liu. Learning to prompt for vision-language models. *International Journal of Computer Vision*, 130(9):2337–2348, 2022. 8
- [56] Xiaohan Zou, Changqiao Wu, Lele Cheng, and Zhongyuan Wang. Tokenflow: Rethinking fine-grained cross-modal alignment in vision-language retrieval. *arXiv preprint arXiv:2209.13822*, 2022. 3, 8, 13